Letters

Impedance Analysis of SOGI-FLL-Based Grid Synchronization

Hao Yi, *Member, IEEE*, Xiongfei Wang, *Member, IEEE*, Frede Blaabjerg, *Fellow, IEEE*, and Fang Zhuo, *Member, IEEE*

***Abstract*—The latest research has pointed out that the phase-locked loop (PLL) plays an important role in shaping the impedance of grid-connected converters, yet most of the works so far merely focus on the synchronous reference-frame PLL. Alternatively, this letter presents the impedance analysis of the second-order generalized integrator frequency-locked loop (SOGI-FLL), which has been introduced for realizing grid synchronization in the stationary reference frame. The influences of the voltage perturbation on the estimated phase and further on the output current are revealed for the grid-connected converter using the SOGI-FLL. The frequency-coupling effect of the SOGI-FLL is also identified and verified in the experimental tests.**

***Index Terms*—Grid-connected converter, impedance analysis, phase-locked loop, second-order generalized integrator frequency-locked loop.**

I. Introduction

IMPEDANCE modeling is an important tool for analyzing the power quality and stability of grid-connected converters [1]–[3]. It has recently been found that the phase-locked loop (PLL) plays an important role in shaping the converter output impedance [4]–[7]. Basically, the PLL is employed to track the phase of the grid voltage vector in order to control the converter output current and power. Given a perturbation imposed at the grid voltage, the measured phase of the PLL will have an angle error $\Delta\theta$ superposed to the ideal grid phase θ_1. This $\Delta\theta$ will then be transferred to the current control loop through coordinate transformations, and consequently affect the control output impedance.

A number of research efforts have been made to address the impacts of $\Delta\theta$ on the synchronous-reference-frame (SRF) current control [4], [5]. It is shown that a negative resistor is introduced along the q-axis, which may destabilize the grid–converter interaction [8]. Besides the SRF impedance model, a stationary-reference-frame impedance model has also been reported in [6], which formulates the system dynamics in the positive and negative sequence by means of the harmonic linearization principle [9]. However, the frequency-coupling effect caused by $\Delta\theta$ is overlooked in this sequence-domain model, which, as recently identified in [7], may result in the inaccurate stability prediction.

These research works have unveiled the dynamic effect of the PLL on the grid-connected converters, yet most of them merely focus on the dynamics of the SRF-PLL. In contrast, the second-order generalized integrator frequency-locked loop (SOGI-FLL), which realizes the grid synchronization directly in the stationary reference frame, is often overlooked in the impedance modeling and analysis [6], [10].

This letter, thus, attempts to fill in this gap by developing the impedance model of the grid-connected converter using the SOGI-FLL for grid synchronization. The impedance shaping effect and the associated frequency-coupling dynamics of the SOGI-FLL-based grid synchronization are explicitly analyzed, which is then validated in the experiments. The results confirm that the developed model provides a theoretical basis for addressing the dynamic impacts of the stationary-reference-frame grid synchronization technique.

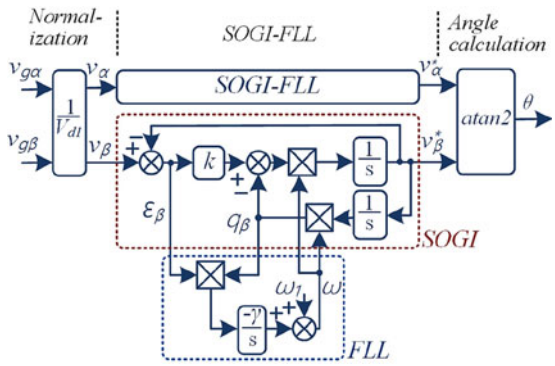

Fig. 1. Block diagram of the SOGI-FLL-based grid synchronization, where $v_{g\alpha}$ and $v_{g\beta}$ represent the grid voltage before normalization.

II. Small-Signal Modeling of SOGI-FLL-Based Grid Synchronization

A. System Description

Fig. 1 shows the block diagram of the SOGI-FLL-based grid synchronization for a three-phase grid-connected converter. This approach is implemented in the stationary $\alpha\beta$ -frame and it consists of three parts:

1) the normalization of the positive-sequence fundamental-frequency voltage magnitude (V_{d1});
2) the SOGI-FLL for the frequency-adaptive filtering;
3) the "atan2" for the phase angle calculation based on the filtered fundamental voltage component.

Manuscript received November 9, 2016; revised December 19, 2016; accepted February 21, 2017. Date of publication February 23, 2017; date of current version May 9, 2017. This work was supported in part by the National Natural Science Foundation of China under Grant 51507132, and in part by the Power Electronics Science and Education Development Program of Delta Environmental and Educational Foundation under Grant DREG2015018.

H. Yi and F. Zhuo are with the State Key Laboratory of Electrical Insulation and Power Equipment, Xi'an Jiaotong University, Xi'an 710049, China (e-mail: yi_hao@xjtu.edu.cn; zffz@mail.xjtu.edu.cn).

X. Wang and F. Blaabjerg are with the Department of Energy Technology, Aalborg University, Aalborg 9220, Denmark (e-mail: xwa@et.aau.dk; fbl@et.aau.dk).

Color versions of one or more of the figures in this letter are available online at http://ieeexplore.ieee.org.

Digital Object Identifier 10.1109/TPEL.2017.2673866

The small-signal model of the stationary-reference-frame grid synchronization method can be derived by linearizing the SOGI-FLL and the "atan2" on the small perturbation in the grid voltage vector. And the imposed small perturbation is a single balanced harmonic voltage, in positive sequence or negative sequence. Moreover, it is also worth noting that all the frequency-domain expressions define $s = j\omega$, where $j\omega > 0$ represents the positive-sequence components and $j\omega < 0$ for the negative-sequence components.

B. Linearizing SOGI-FLL

As shown in Fig. 1, the α-axis and β-axis are symmetrical at the part of SOGI-FLL; hence, only the β-axis modeling is introduced here. According to the block diagram, SOGI has the following relations:

$$v_\beta^* = \frac{k\omega s}{s^2 + k\omega s + \omega^2} v_\beta = \mathrm{BPF}_\omega \cdot v_\beta \tag{1}$$

$$q_\beta^* = \frac{k\omega^2}{s^2 + k\omega s + \omega^2} v_\beta = k \cdot \mathrm{LPF}_\omega \cdot v_\beta \tag{2}$$

where v_β is the input of the SOGI, while v_β^* and q_β^* are the in-phase-output and quadrature-phase-output of the SOGI, respectively, k is the gain, BPF_ω and LPF_ω represent the second-order band-pass filter (BPF) and low-pass filter (LPF) at the angular frequency ω, respectively. And ω is the output of the FLL, which is the fundamental frequency (ω_1) with the ideal grid.

However, given a small perturbation to the grid voltage, the β-axis voltage becomes (3) in the frequency domain.

$$v_\beta = V_{\beta 1}[\omega_1] + \Delta v_{\beta h}. \tag{3}$$

Then, errors appear in the outputs v_β^* and ω, which are

$$v_\beta^* = V_{\beta 1}^*[\omega_1] + \Delta v_{\beta h}^* \tag{4}$$

$$\omega = \omega_1 + \Delta\omega_h \tag{5}$$

where $V_{\beta 1}[\omega_1]$ and $V_{\beta 1}^*[\omega_1]$ represent the fundamental components of v_β and v_β^*, respectively; $\Delta v_{\beta h}^*$ and $\Delta\omega_h$ are the voltage error and frequency error caused by the perturbation $\Delta v_{\beta h}$.

Then, substituting (3)–(5) into (1) and neglecting the second- and higher order terms of the errors, the small-signal dynamics of the β-axis output voltage can be given by

$$V_{\beta 1}^*[\omega_1] + \Delta v_{\beta h}^* = \underbrace{\frac{k\omega_1 s}{D_1} V_{\beta 1}[\omega_1]}_{V_{\beta 1}^*[\omega_1]} + \frac{k\omega_1 s}{D_1}\Delta v_{\beta h} - \frac{2\omega_1 \Delta\omega_h}{D_1} V_{\beta 1}^*[\omega_1] + k\Delta\omega_h s \underbrace{(V_{\beta 1}[\omega_1] - V_{\beta 1}^*[\omega_1])}_{0} \tag{6}$$

where $D_1 = s^2 + k\omega_1 s + \omega_1^2$, and $k\omega_1 s/D_1$, defined as $\mathrm{BPF}_{\omega 1}$, is a typical BPF at the fundamental frequency ω_1.

Since $\mathrm{BPF}_{\omega 1}$ gives no attenuation on $V_{\beta 1}[\omega_1]$, relationships (7) exist, which imply the steady-state operating point at the fundamental frequency

$$\begin{cases} V_{\beta 1}^*[\omega_1] = V_{\beta 1}[\omega_1] \cdot BPF_{\omega 1} \\ V_{\beta 1}^*[\omega_1] = V_{\beta 1}[\omega_1] = V_1 \end{cases} \tag{7}$$

where $V_1 = 1$ in the steady state because of the normalization shown in Fig. 1.

Considering relations (7), (6) becomes

$$\Delta v_{\beta h}^* = \mathrm{BPF}_{\omega 1} \cdot \Delta v_{\beta h} - 2\mathrm{LPF}_{\omega 1} \cdot \frac{\Delta\omega_h}{\omega_1}. \tag{8}$$

Expression (8) indicates that the SOGI provides not only an ideal $\mathrm{BPF}_{\omega 1}$ for the perturbation $\Delta v_{\beta h}$, but also an $\mathrm{LPF}_{\omega 1}$ filtering the frequency error $\Delta\omega_{\mathrm{h}}$. Since $\Delta\omega_h$ comes from the FLL and is caused by $\Delta v_{\beta h}$, FLL should also be linearized.

According to Fig. 1, the transfer function of FLL is

$$\omega = -\frac{\gamma}{s}(v_\beta - v_\beta^*) \cdot q_\beta = -\frac{\gamma}{s}(1 - \mathrm{BPF}_\omega) \cdot k \cdot \mathrm{LPF}_\omega \cdot v_\beta. \tag{9}$$

Similar linearizing process can be performed, which substitutes (3) and (5) into (9), and then applies harmonic linearization. In this way, we get

$$\Delta\omega_h = \underbrace{-\frac{2\gamma k(s^2 + \omega_1^2)\omega_1^2}{sD_1^2 + 2sD_1\omega_1(ks + 2\omega_1) + 2k\gamma\omega_1(s^2 + 2\omega_1^2)}}_{H(s)} \cdot \Delta v_{\beta h}. \tag{10}$$

Further substituting (10) into (8), the linearized small-signal model of the SOGI-FLL is obtained as

$$\Delta v_{\beta h}^* = \underbrace{\left(\mathrm{BPF}_{\omega 1} + \frac{2}{\omega_1}\mathrm{LPF}_{\omega 1} \cdot H(s)\right)}_{G_{\mathrm{SOGI}}(s)} \cdot \Delta v_{\beta h}. \tag{11}$$

It is noted that the α-axis model has the same form as (11) due to the symmetry yet with only a different subscript αh.

C. Linearizing "atan2"

To calculate the phase angle of the grid voltage, arctangent is employed in form of "atan2" following the SOGI-FLL, as shown in Fig. 1. It gives an angle at range of $[-\pi, \pi]$ with definition that

$$a\tan 2(v_\beta^*, v_\alpha^*) = \begin{cases} \arctan(v_\beta^*/v_\alpha^*) & v_\alpha^* > 0 \\ \arctan(v_\beta^*/v_\alpha^*) + \pi & v_\alpha^* < 0, v_\beta^* \geq 0 \\ \arctan(v_\beta^*/v_\alpha^*) - \pi & v_\alpha^* < 0, v_\beta^* < 0 \\ +\pi/2 & v_\alpha^* = 0, v_\beta^* > 0 \\ -\pi/2 & v_\alpha^* = 0, v_\beta^* < 0 \end{cases}. \tag{12}$$

For small-signal modeling, "atan2" can be simply regarded as "arctan," and it can be linearized as

$$\theta(t) = \theta_1(t) + \frac{\partial \arctan(v_\beta^*/v_\alpha^*)}{\partial v_\alpha^*} \underbrace{(v_\alpha^*(t) - V_{\alpha 1}^*(t))}_{\Delta v_{\alpha h}^*(t)} + \frac{\partial \arctan(v_\beta^*/v_\alpha^*)}{\partial v_\beta^*} \underbrace{(v_\beta^*(t) - V_{\beta 1}^*(t))}_{\Delta v_{\beta h}^*(t)}. \tag{13}$$

Considering that $\Delta\theta(t) = \theta(t) - \theta_1(t)$, (13) becomes

$$\Delta\theta(t) = \frac{-V_{\beta 1}^*(t) \cdot \Delta v_{\alpha h}^*(t) + V_{\alpha 1}^*(t) \cdot \Delta v_{\beta h}^*(t)}{V_{\alpha 1}^{*2}(t) + V_{\beta 1}^{*2}(t)}. \tag{14}$$

Since $V_\alpha^* 1(t)$ and $V_{\beta 1}^*(t)$ are the ideal fundamental components in the outputs of SOGI-FLL in the α-axis and β-axis, respectively, they are simply set as

$$\begin{cases} V_{\alpha 1}^*(t) = V_1 \cos(\omega_1 t) \\ V_{\beta 1}^*(t) = V_1 \sin(\omega_1 t) \end{cases}. \tag{15}$$

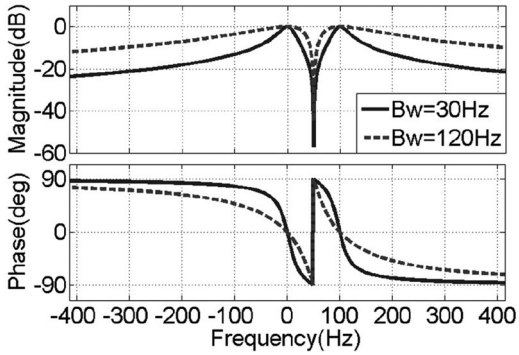

Fig. 2. Frequency-response diagram of $G_{\mathrm{SOGI}}(s-j\omega_1)$ for describing the relationship of $\Delta\theta(s-j\omega_1)$ and $\Delta v_{\beta h}(s)$ [see (22)].

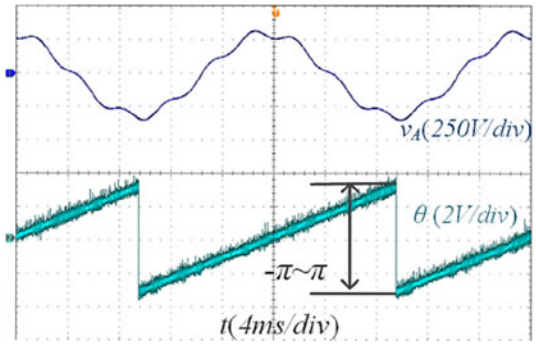

Fig. 3. Phase angle estimated by the SOGI-FLL-based grid synchronization, where θ is in its actual values.

Then, (14) can be further expressed as (16) by considering that $V_1 = 1$

$$\Delta\theta(t) = -\Delta v^*_{\alpha h}(t)\cdot\sin(\omega_1 t) + \Delta v^*_{\beta h}(t)\cdot\cos(\omega_1 t). \tag{16}$$

Afterwards, employing Euler equations of

$$\begin{cases}\sin(\omega_1 t) = -j\left(e^{j\omega_1 t} - e^{-j\omega_1 t}\right)/2\\ \cos(\omega_1 t) = \left(e^{j\omega_1 t} + e^{-j\omega_1 t}\right)/2\end{cases} \tag{17}$$

and then applying Laplace transformation, (16) turns to

$$\begin{aligned}\Delta\theta(s) = \frac{1}{2}[&j\Delta v^*_{\alpha h}(s-j\omega_1) - j\Delta v^*_{\alpha h}(s+j\omega_1)\\ &+ \Delta v^*_{\beta h}(s-j\omega_1) + \Delta v^*_{\beta h}(s+j\omega_1)].\end{aligned} \tag{18}$$

Since the $\alpha\beta$ components of a balanced voltage perturbation keep the frequency-domain relation [11] of

$$\Delta v^*_{\alpha h}(s) = j\Delta v^*_{\beta h}(s) \tag{19}$$

expression (18) can be simplified as

$$\Delta\theta(s) = -j\Delta v^*_{\alpha h}(s+j\omega_1) = \Delta v^*_{\beta h}(s+j\omega_1). \tag{20}$$

Finally, substituting (11) into (20), the linearized small-signal model of the SOGI-FLL-based grid synchronization can be obtained as

$$\begin{aligned}\Delta\theta(s) &= -jG_{\mathrm{SOGI}}(s)\cdot\Delta v_{\alpha h}(s+j\omega_1)\\ &= G_{\mathrm{SOGI}}(s)\cdot\Delta v_{\beta h}(s+j\omega_1).\end{aligned} \tag{21}$$

The model in (21) reveals the impact of the voltage perturbation on $\Delta\theta$, and 90° phase difference between α-axis and β-axis model is due to the relation (19). According to the derivation, the SOGI-FLL gives a small-signal model G_{SOGI}, while the linearized "atan2" introduces a fundamental-frequency shift to $\Delta v_{\alpha h}$ and $\Delta v_{\beta h}$, as given in (21).

III. Impact on Measured Phase

A fundamental-frequency shift can be applied to (21) to directly observe the impact of the voltage perturbation on $\Delta\theta$, which is

$$\frac{\Delta\theta(s-j\omega_1)}{\Delta v_{\beta h}(s)} = G_{\mathrm{SOGI}}(s-j\omega_1). \tag{22}$$

It reveals a fact that, with the SOGI-FLL-based grid synchronization, a voltage perturbation $\Delta v_h(j\omega)$ will introduce an angle error $\Delta\theta$, varying at a shifted frequency $(j\omega - j\omega_1)$. The corresponding frequency response is shown in Fig. 2, where the grid fundamental frequency is 50 Hz and the negative frequency represents the negative-sequence component. And moreover, two values of the synchronization loop bandwidth (Bw), which is defined as the bandwidth of $\mathrm{BPF}_{\omega 1}$ in (11), are compared in the figure.

It can be seen that G_{SOGI} mainly performs as a BPF, even though there is an additional term in (11). That is because this term is introduced by $\Delta\omega$, while, with the small voltage perturbation, $\Delta\omega$ is quite small and consequently has quite limited influence.

To verify these features, the SOGI-FLL scheme is implemented in the lab to estimate the phase of a three-phase voltage. The three-phase voltage is generated by a programmable ac source and contains the fundamental component at 50 Hz/220 V mixed with a specific perturbation at 10% magnitude of the fundamental. For simplicity, only phase-A voltage (v_A) is displayed in the test results. Moreover, to clearly show the impacts on $\Delta\theta$, larger synchronization loop bandwidth, which is $\mathrm{Bw} = 120\,\mathrm{Hz}$, is selected in the test. And corresponding results, θ and $\Delta\theta$ are output by a D/A converter for displaying.

As shown in Fig. 3, the grid synchronization with SOGI-FLL gives θ at the range of $[-\pi, +\pi]$ due to "atan2." Since perturbation is given to the grid voltage, shown as the waveform v_A in Fig. 3, $\Delta\theta$ exists in θ, although it is quite small.

To examine the details, $\Delta\theta$ is extracted by subtracting the phase of the ideal fundamental voltage (θ_1) from the measured θ, which is then amplified 100 times larger before output by a D/A converter. By doing so, $\Delta\theta$ can be easily observed and analyzed in the test results, but it is worth keeping in mind that this $\Delta\theta$ is actually 100 times larger than its actual values.

In this way, Fig. 4(a)–(c) depicts the test results about $\Delta\theta$ caused by voltage perturbations at the positive-sequence sixth-order $(j6\omega_1)$, the negative-sequence sixth-order $(-j6\omega_1)$, and the positive-sequence 25 Hz $(j0.5\omega_1)$, respectively.

In line with the theoretical analysis, the voltage perturbation $\Delta v_h(j\omega)$ will bring the angle error $\Delta\theta(j\omega - j\omega_1)$, which is $\Delta\theta$ varying at the positive fifth-order $(j6\omega_1 - j\omega_1)$ in Fig. 4(a), the negative seventh-order $(-j6\omega_1 - j\omega_1)$ in Fig. 4(b), and the negative 25 Hz $(j0.5\omega_1 - j\omega_1)$ in Fig. 4(c). Moreover, reducing the synchronization loop bandwidth in the tests can suppress down $\Delta\theta$ for any kind of perturbation, which is consistent with the frequency responses shown in the Fig. 2.

IV. Impedance Analysis of Grid-Connected Voltage Source Converter (VSC)

The model in (21) is the basis of the impedance analysis for a grid-connected converter that employs SOGI-FLL for grid synchronization. Taking a three-phase VSC with an SRF-PI current controller as an

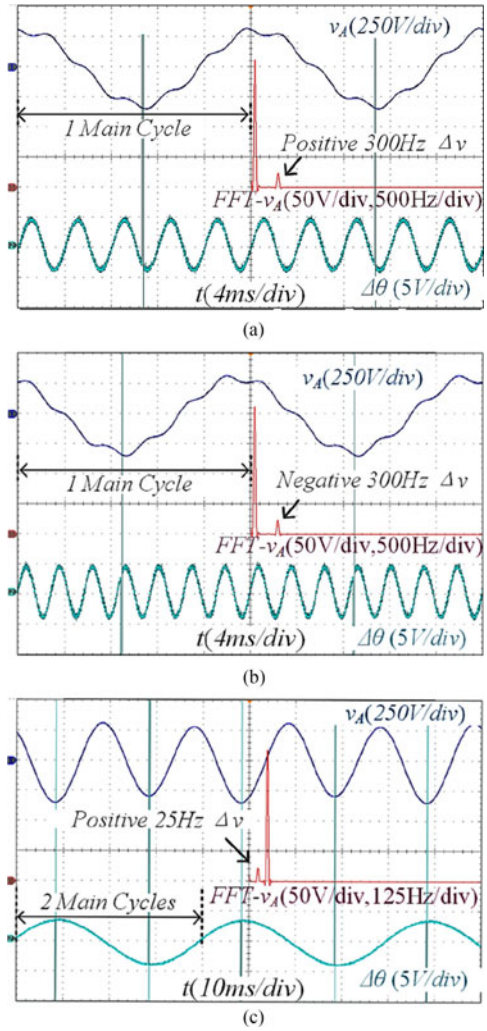

Fig. 4. Test results of the impact of $\Delta v_h(j\omega)$ on $\Delta\theta(j\omega - j\omega_1)$, where $\Delta\theta$ is magnified at 100 times larger than its actual values. (a) With positive sixth-order perturbation; (b) with negative sixth-order perturbation; (c) with positive 25-Hz perturbation.

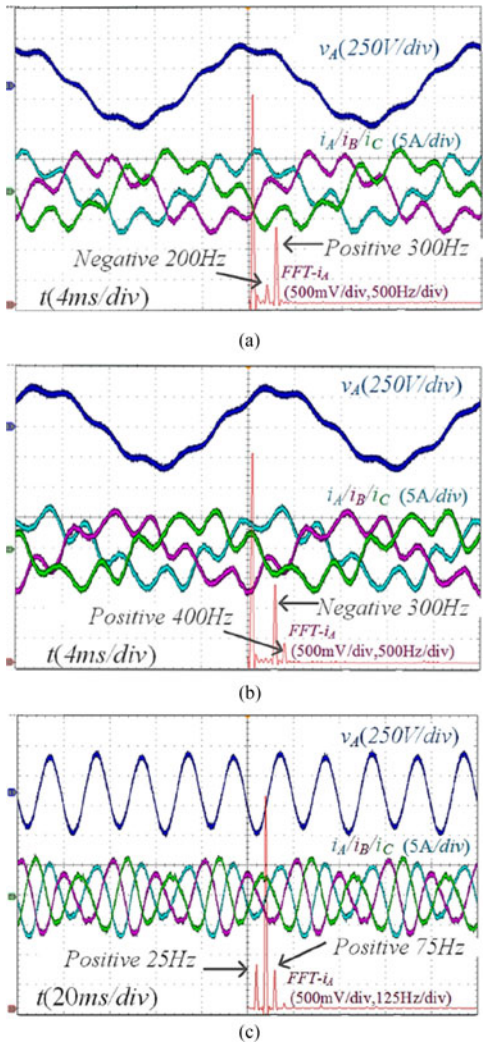

Fig. 5. Test results for frequency-coupling current due to perturbation Δv_h. (a) For positive-sequence sixth-order perturbation; (b) for negative-sequence sixth-order perturbation; (c) for positive-sequence 25-Hz perturbation.

TABLE I
MAIN PARAMETERS OF THE TEST SETUP

AC voltage (1st)	220 V/50 Hz	DC voltage	$V_{\mathrm{DC}} = 730$ V
Perturbations	10% in mag.	Line inductor	$L = 3$ mH
Switch frequency	$f_s = 10$ kHz	bandwidth	$Bw = 120$ Hz
d-axis ref.	$i_d^{\mathrm{ref}} = 5$ A	q-axis ref.	$i_q^{\mathrm{ref}} = 0$

example, its harmonic impedance model in the $\alpha\beta$ frame is

$$\begin{cases} \Delta i_{\alpha\beta,h}(s) = \left[-X(s) + Z(s)\cdot\dfrac{G_{\mathrm{SOGI}}(s-j\omega_1)}{V_{d1}}\right]\cdot\Delta v_{\alpha\beta,h}(s) \\ \Delta i_{\alpha\beta,h}[-(s-j2\omega_1)] = Y(s)\cdot\underbrace{\dfrac{G_{\mathrm{SOGI}}(s-j\omega_1)}{V_{d1}}\cdot\Delta v_{\alpha\beta,h}(s)}_{\Delta\theta(s-j\omega_1)} \end{cases} \tag{23}$$

where X(s), Z(s), and Y(s) are expressed in the appendix.

Please note that the derivation of (23) is similar to the work in [7]. The differences are that SOGI-FLL is employed for grid synchronization, and the sign of frequency is used to distinguish the positive sequence and the negative sequence. Consequently, two equations, instead of four, are enough to describe the impedance model.

The model in (23) reveals how G_{SOGI} affects the output impedance of VSC. It implies that the voltage perturbation $\Delta v_h(j\omega)$ will not only bring in the harmonic current at the frequency of perturbation but also cause a coupling current at the frequency $[-(j\omega - j2\omega_1)]$, which is in the opposite sequence for the frequency with a double-fundamental-reducing shift from the frequency of perturbation.

This frequency-coupling dynamics is firstly pointed out for the condition with SRF-PLL [7]. And according to (23), this dynamics still exists when the stationary-reference-frame SOGI-FLL is employed for grid synchronization. As indicated by the lower part of (23), the impedance of the frequency coupling is directly related to $\Delta\theta$. Therefore, this frequency-coupling dynamics can reflect and validate the features of the developed G_{SOGI}.

To verify the analysis, a three-phase VSC with constant dc-link voltage is connected to a programmable ac source in the lab and is commanded to inject fundamental current to the source with an SRF-PI current controller. SOGI-FLL is employed for grid synchronization and detailed parameters are listed in Table I. Please note that the 120-Hz synchronization loop bandwidth is selected to better show the

influences of $\Delta\theta$, and it did not introduce instability issue because of the low grid impedance.

In the tests, the positive-sequence sixth-order perturbation $(j6\omega_1)$, negative-sequence sixth-order perturbation $(-j6\omega_1)$, and positive-sequence 25-Hz perturbation $(j0.5\omega_1)$, each with 10% magnitude of the fundamental, are given to the ac voltage separately. The frequency couplings are observed at the frequencies predicted by (23). They are the coupling current at the negative-sequence fourth-order $[-(j6\omega_1 - j2\omega_1)]$ in the Fig. 5(a), at the positive-sequence eight-order $[-(-j6\omega_1 - j2\omega_1)]$ in the Fig. 5(b), and at the positive-sequence 75 Hz $[-(j0.5\omega_1 - j2\omega_1)]$ in the Fig. 5(c), respectively.

The frequency coupling also exists even with the perturbations at any other frequencies. And taking sixth-order perturbation as an example further illustrates that the resulting harmonic components are not the characteristic harmonic components of the three-phase grid-connected VSC, hence giving better validation about the topic.

Moreover, reducing the synchronization loop bandwidth can effectively suppress the magnitude of the frequency-coupling current in the tests. All these results validate the model and analysis in this letter.

V. Conclusion

This letter presents a detailed derivation of the small-signal model of the SOGI-FLL-based grid synchronization, which describes the impact of the voltage perturbation on $\Delta\theta$ as a fundamental-frequency-shifted BPF. The model provides a theoretical basis for addressing the dynamic impacts of this stationary-reference-frame grid synchronization technique. And based on the model, its impedance shaping effects and frequency-coupling dynamics are analyzed in the frequency domain and validated through experimental tests.

Appendix

$$X(s) = 1/\left(sL + V_{\mathrm{DC}} \cdot F(s - j\omega_1)\right) \tag{A.1}$$

$$Z(s) = X(s)\left(V_{\mathrm{DC}} \cdot F(s - j\omega_1) \cdot (i_d^{\mathrm{ref}} + j i_q^{\mathrm{ref}})\right)/2 \tag{A.2}$$

$$Y(s) = X(s - j2\omega_1)\left(V_{\mathrm{DC}} \cdot F(s - j\omega_1) \cdot (i_d^{\mathrm{ref}} - j i_q^{\mathrm{ref}})\right)/2 \tag{A.3}$$

where *F(s)* represents an SRF-PI current controller.

Reference

[1] L. Harnefors, M. Bongiorno, and S. Lundberg, "Input-admittance calculation and shaping for controlled voltage-source converters," *IEEE Trans. Ind. Electron.*, vol. 54, no. 6, pp. 3323–3334, Dec. 2007.

[2] L. Harnefors, X. Wang, A. G. Yepes, and F. Blaabjerg, "Passivity-based stability assessment of grid-connected VSCs—An overview," *IEEE J. EmergencySel. Top. Power Electron.*, vol. 4, no. 1, pp. 116–125, Mar. 2016.

[3] M. Cespedes and J. Sun, "Impedance shaping of three-phase grid-parallel voltage-source converters," in *Proc. IEEE Appl. Power Electron. Conf. Expo.*, Feb. 2012, pp. 754–760.

[4] L. Harnefors, "Modelling of three-phase dynamic systems using complex transfer functions and transfer matrices," *IEEE Trans. Ind. Electron.*, vol. 54, no. 4, pp. 2239–2248, Aug. 2007.

[5] B. Wen, D. Boroyevich, R. Burgos, P. Mattavelli, and Z. Shen, "Analysis of D-Q small-signal impedance of grid-tied inverters," *IEEE Trans. Power Electron.* vol. 31, no. 1, pp. 675–687, Jan. 2016.

[6] M. Cespedes and J. Sun, "Impedance modelling and analysis of grid-connected voltage-source converters," *IEEE Trans. Power Electron.*, vol. 29, no. 3, pp. 1254–1261, Mar. 2014.

[7] M. K. Bakhshizadeh, X. Wang, F. Blaabjerg, L. Kocewiak, C. L. Bak, and B. Hesselbak, "Coupling in phase domain impedance modelling of grid-connected converters," *IEEE Trans. Power Electron.*, vol. 31, no. 10, pp. 6792–6796, Oct. 2016.

[8] B. Wen, D. Dong, D. Boroyevich, R. Burgos, P. Mattavelli, and Z. Shen, "Impedance-based analysis of grid-synchronization stability for three-phase paralleled converters," *IEEE Trans. Power Electron.*, vol. 31, no. 1, pp. 26–38, Apr. 2016.

[9] J. Sun, "Small-signal methods for AC distributed power systems—A review," *IEEE Trans. Power Electron.*, vol. 24, no. 11, pp. 2545–2554, Nov. 2009.

[10] C. Zhang, X. Wang, F. Blaabjerg, W. Wang, and C. Liu, "The influence of phase-locked loop on the stability of single-phase grid-connected inverter," *in Proc. IEEE Energy Convers. Congr. Expo.*, Sep. 20–24, 2015, pp. 4737–4744.

[11] P. Rodriguez, A. Luna, R. S. Munoz-Aguilar, I. Etxeberria-Otadui, R. Teodorescu, and F. Blaabjerg, "A stationary reference frame grid synchronization system for three-phase grid-connceted power converters under adverse grid conditions," *IEEE Trans. Power Electron.*, vol. 27, no. 1, pp. 99–112, Jan. 2012.